Adsorption Behaviors and Mechanisms of Cu^{2+}, Zn^{2+} and Pb^{2+} by Magnetically Modified Lignite

Junzhen Di
Liaoning Technical University
Zhen Ruan (zhenruanlntu@126.com)
Liaoning Technical University
Siyi Zhang
Liaoning Technical University

Research Article

Keywords: acid mine wastewater (AMD), magnetically modified lignite (MML), Fourier transform infrared spectrometer (FTIR).

Posted Date: October 4th, 2021

DOI: https://doi.org/10.21203/rs.3.rs-936414/v1

Version of Record: A version of this preprint was published at Scientific Reports on January 26th, 2022. See the published version at https://doi.org/10.1038/s41598-022-05453-y.

Abstract

In order to solve the problems of high content of Cu^{2+}, Zn^{2+} and Pb^{2+} in acid mine wastewater (AMD), and limited adsorption capacity of lignite, the lignite was used as raw material to prepare magnetically modified lignite (MML), and adsorption performance of lignite and MML on Cu^{2+}, Zn^{2+} and Pb^{2+} was investigated by static beaker experiment and dynamic continuous column experiment. At the same time, the adsorption mechanism was revealed by means of scanning electron microscopy (SEM), X-ray diffractometer (XRD) and Fourier transform infrared spectrometer (FTIR). The results showed that the adsorption processes of lignite and MML on heavy metal ions were more consistent with the Langmuir model, obeying the quasi first-order model and quasi second-order model, respectively. In addition, the intraparticle diffusion model indicated that the adsorption processes were jointly controlled by multiple adsorption stages. The dynamic continuous column experiments showed that the average removal rates of Cu^{2+}, Zn^{2+} and Pb^{2+} were 78.00%, 76.97% and 78.65% for lignite and 82.83%, 81.57% and 83.50% for MML, respectively. Compared with lignite, the adsorption effect of MML was better. From SEM, XRD and FTIR tests, it can be seen that the magnetic modification process successfully loads Fe_3O_4 onto the surface of lignite, making the surface morphology rougher, and the adsorption process of MML on Cu^{2+}, Zn^{2+} and Pb^{2+} is related to the O-H stretching vibration of carboxylic acid ions and Fe-O stretching vibration of Fe_3O_4 particles.

Introduction

During the mining process, coal can change from the original reducing environment to oxidizing environment, and the sulfide in it can produce a large amount of acid substances under the action of bacteria and oxygen, which can dissolve in water to form acid mine wastewater (AMD)[1]. AMD has multiple hazards to the natural environment, specifically manifested as low pH, high sulfate concentration, and high heavy metal ion content[2]. In addition, Cu^{2+}, Zn^{2+}, Pb^{2+} and other heavy metal ions cannot be biodegraded or metabolized. After a series of food chain conduction, these metal elements are easily ingested into the human body, causing many health threats[3,4]. Therefore, it is necessary to find some reliable methods to remove heavy metal ions such as Cu^{2+}, Zn^{2+} and Pb^{2+} from AMD.

The treatment methods of heavy metal pollution in AMD mainly include neutralization precipitation method, microbiological method, wetland method and adsorption method, etc.[5–8]. The neutralization sedimentation method will produce a large amount of sludge products during the treatment of pollution, which will cause new environmental problems and treatment costs [7]. The microbiological method has high processing cost and harsh reaction conditions. The wetland method has low investment cost, but it covers a large area and is limited by time. Compared with the above methods, the adsorption method has the advantages of simple operation and high efficiency, and is considered as the preferred method to treat heavy metal ions in wastewater[9,10]. Activated carbon is a commonly used adsorbent in the adsorption method, which can adsorb heavy metal ions in wastewater very effectively, but the expensive raw material cost limits its use. Therefore, looking for an economical and reliable adsorption material has become a hot topic in the current field. Lignite is a natural adsorbent material, which is rich in humic acid and has oxygen-producing functional groups such as carboxyl, hydroxyl, and methoxy groups, and has a certain adsorption effect on heavy metal ions in solution[11–13].Dinesh Mohan et al.[14] have demonstrated that lignite can be used as a substitute for activated carbon. However, primary lignite has a complex composition and a single void structure, which has limited adsorption capacity for heavy metal ions. Therefore, in order to improve the adsorption performance of lignite, many scholars have modified the lignite. Yang Qiuyun et al.[15] conducted a chemical oxidation modification study on lignite and found that the adsorption capacity of cadmium by nitrified lignite was increased by 20.18%-22.62%. Zhang Huaicheng et al.[16] investigated the acid-base modification of lignite and found that the adsorption capacity of alkalized lignite and sulfonated lignite was significantly improved by 6.6 and 3.6 times, respectively, compared to untreated lignite. Di Junzhen et al.[17] proposed microbial modification of lignite, and the study found that the removal rate of Cu^{2+} and Zn^{2+} by pseudomonas aeruginosa modified lignite was increased by more than 15%. In recent years, the use of magnetically modified materials as adsorbents to treat heavy metal wastewater has become a research hotspot. Cheng Zihong et al.[18] prepared magnetically modified wood chips using chitosan as a bridging reagent and showed that magnetically modified wood chips were effective materials for the removal of strontium ions from aqueous solutions. Wang Weiping et al.[19] used chemical co-precipitation method to modify sepiolite to study magnetically modified sepiolite for the treatment of heavy metal wastewater, and the results showed that the increase in specific surface area of magnetically modified sepiolite was

beneficial to the adsorption of heavy metal ions Cu^{2+}, Pb^{2+}, and Cd^{2+}. Up to now, there are few studies on magnetic modification of lignite to investigate the properties of magnetically modified lignite (MML) for heavy metal ion adsorption.

In this paper, lignite was used as raw material to prepare magnetically modified lignite by chemical co-precipitation method, and static beaker experiment and dynamic continuous column experiment were used to compare the treatment effects of lignite and MML on Cu^{2+}, Zn^{2+}, and Pb^{2+} in AMD. The adsorption characteristics of lignite and MML on Cu^{2+}, Zn^{2+} and Pb^{2+} in AMD were analyzed based on the test of the effect of initial concentration of heavy metal ions in the solution, adsorption isotherm and adsorption kinetics test. At the same time, SEM, XRD and FTIR were used to reveal the adsorption mechanism of lignite and MML to adsorb Cu^{2+}, Zn^{2+}, and Pb^{2+} in AMD.

Results And Discussion

Effect of different initial concentrations of metal ions on adsorption

The adsorption capacity and removal rates of lignite and MML for different initial concentrations of metal ions are shown in Fig. 1. The adsorption of heavy metal ions by lignite and MML increases with the increase of initial concentration (Fig. 1). This is due to the fact that the higher the initial concentration of metal ions, the higher the chance of collision with the adsorption sites on the surface of the adsorbent material and the better mass transfer driving force, which is conducive to reducing the mass transfer resistance and increasing the adsorption amount[20]. The removal rate of lignite and MML for metal elements decreases with increasing initial concentration, and the slope of the removal rate curve increases significantly near the initial concentration of Cu^{2+} at 30 mg/L, Zn^{2+} at 30 mg/L, and Pb^{2+} at 50 mg/L. This is because for a fixed amount of adsorbent material, the number of adsorption sites on its surface is limited and the adsorption effect will reach the best adsorption at a certain metal ion concentration.

Comparing the adsorption effects of lignite and MML on heavy metal ions, it can be seen that the adsorption capacity and removal rates of Cu^{2+}, Zn^{2+} and Pb^{2+} by MML were higher than those by lignite at the same concentrated metal ion degree. In the initial concentration range of 10–90 mg/L, the removal rates of Cu^{2+} and Zn^{2+} by lignite and MML showed similar trends, and the difference in removal rates tended to increase. In contrast, the removal rate of Pb^{2+} by MML in the range of 10–50 mg/L was almost constant with increasing initial concentration, indicating that Pb^{2+} in AMD was well removed by MML in this range. In addition, the difference of adsorption of Cu^{2+}, Zn^{2+} and Pb^{2+} between MML and lignite in the range of initial concentration 10–90 mg/L increased with the increase of initial concentration. This phenomenon indicates that MML has greater adsorption potential than lignite when the concentration of heavy metal ions in AMD solution is higher.

Adsorption isotherm

To clarify the mechanism of Cu^{2+}, Zn^{2+} and Pb^{2+} adsorption by lignite and MML, the Langmuir model and Freundlich model were used to fit the experimental data based on the adsorption isotherm principle.

The Langmuir model assumes that monolayer adsorption occurs on the uniform adsorbent surface, with no interaction between adsorbates. The Langmuir model is expressed in the following form:

$$\frac{C_e}{q_e} = \frac{C_e}{q_m} + \frac{1}{\left(K_L q_m\right)} \quad (1)$$

Where q_m and q_e are the maximum adsorption capacity and the adsorption capacity at equilibrium (mg/g), respectively, C_e is the adsorbate concentration in solution at equilibrium(mg/L), and K_L is the Langmuir adsorption constant (L/mg). The values of q_m and K_L can be calculated by a linear relationship. In addition, the equilibrium constant R_L of the Langmuir model can be used to describe the adsorption effect of the adsorption process.The R_L equation is of the following form:

$$R_L = 1 / \left(1 + K_L C_0\right) \quad (2)$$

where C_0 is the initial concentration of metal ions. The value R_L<1 indicates good adsorption performance.

Based on multilayer adsorption on non-homogeneous surfaces, the empirical Freundlich equation without assumptions is expressed in the following form:

$$\ln q_e = \ln K_F + \frac{1}{n} \ln C_e \quad (3)$$

The adsorption isotherms and corresponding parameters of Cu^{2+}, Zn^{2+} and Pb^{2+} adsorption by lignite and MML are shown in Fig. 2 and Table 1, respectively. The correlation coefficient ($R^2 > 0.99$) of the Langmuir model is higher, indicating that the processes of Cu^{2+}, Zn^{2+} and Pb^{2+} adsorption by lignite and MML are more consistent with the Langmuir model (Table 1). On the basis of this result, it can be inferred that the processes of Cu^{2+}, Zn^{2+} and Pb^{2+} adsorption by lignite and MML belong to Langmuir monolayer adsorption, where there is no interaction between the heavy metal ions adsorbed on the surface[20]. Also, R_L was found to be less than 1 by analysis, indicating good adsorption of heavy metal ions[21].The 1/n less than 1 in the Freundlich model also confirms good adsorption conditions[22]. Comparing the parameters of the adsorption isotherms of lignite and MML shows that the correlation coefficient of the Langmuir model for MML is larger,

Table 1
Adsorption isotherm constants for the adsorption of heavy metal ion onto different samples: Lignite; MML.

Metal ion	Adsorption material	Langmuir				Freundlich		
		K_L (L/mg)	q_m (mg/g)	R^2	R_L	K_F (L/mg)	1/n	R^2
Cu^{2+}	Lignite	0.16684	13.36180	0.99576	0.16652	2.26204	0.48950	0.88550
	MML	0.25769	16.21270	0.99926	0.11458	3.47001	0.46680	0.91549
Zn^{2+}	Lignite	0.10161	14.79290	0.99571	0.24702	1.82106	0.54410	0.93473
	MML	0.20573	15.80530	0.99772	0.13943	3.03035	0.47940	0.92316
Pb^{2+}	Lignite	0.09121	17.52740	0.98246	0.17984	1.90594	0.63730	0.92816
	MML	0.25673	18.38700	0.99755	0.07227	8.85303	0.24820	0.85616

which may be due to the homogeneous specific adsorption sites generated during the magnetization process[23]. The maximum adsorption capacities of MML were 16.2127 mg/g, 15.8053 mg/g, and 18.3870 mg/g for Cu^{2+}, Zn^{2+} and Pb^{2+}, respectively, while the maximum adsorption capacities of lignite were 13.3618 mg/g, 14.7929 mg/g, and 17.5274 mg/g for Cu^{2+}, Zn^{2+} and Pb^{2+}, respectively. It indicates that the adsorption capacity of MML is large. In addition, it has been reported that the larger the adsorption capacity of the adsorbent the larger the value of K_F[23]. The value of K_F of MML in this study were larger than those of the original lignite, further confirming that MML is more likely to adsorb heavy metal ions.

Adsorption kinetics

To clarify the adsorption mechanism of lignite and MML, the adsorption kinetics of Cu^{2+}, Zn^{2+} and Pb^{2+} by lignite and MML were analyzed in this paper using quasi first-order kinetic model, quasi second-order kinetic model and intraparticle diffusion model.

Quasi first-order model

Lagergren proposed an adsorption analysis method based on solid adsorption capacity[20], which is the quasi first-order kinetic equation in the following form:

$$\ln\left(q_e - q_t\right) = \ln q_e - k_1 t \quad (4)$$

where q_e and q_t are the amounts of adsorbed metal ions at equilibrium and at time t (mg/g), respectively, and k_1 is the quasi first-order rate constant (min^{-1}).

Quasi second-order model

The quasi second-order kinetic model is based on the assumption that the adsorption rate is controlled by chemisorption[24]. The quasi second-order kinetic model is expressed in the following form:

where q_e and q_t are the amounts of adsorbed metal ions at equilibrium and at time t (mg/g), respectively, and k_2 is the quasi second-order rate constant (min^{-1}).

The results of quasi first-order model and quasi-second-order kinetic fits for the adsorption of Cu^{2+}, Zn^{2+} and Pb^{2+} by lignite and MML are shown in Fig. 3 and Table 2.

From Fig. 3(a) and (b), it can be seen that in the initial stage of adsorption, the slope of the tangent line of the curve is larger, indicating that the adsorption rate of MML and lignite is faster. As the reaction proceeds, the slope gradually decreases. This is due to the fact that there are enough effective adsorption sites on the surface of the adsorbent material in the initial stage, but the adsorption efficiency decreases after the adsorption sites are gradually occupied. As can be seen from Table 2, the quasi first-order kinetic parameters R_2 for the adsorption of Cu^{2+}, Zn^{2+} and Pb^{2+} by lignite were high, indicating that the adsorption process followed the quasi first-order kinetic model and was dominated by physical adsorption. The fitted equations of quasi first-order l kinetics of lignite for Cu^{2+}, Zn^{2+} and Pb^{2+} were: $y = 9.2602*(1 - e^{-0.00607x})$, $y = 10.2839*(1 - e^{-0.00468x})$, and $y = 11.8456*(1 - e^{-0.01265x})$, respectively. However, the quasi second-order kinetic parameter R^2 for the adsorption of heavy metal ions by MML is high, indicating that the adsorption process follows a quasi second-order kinetic model. The adsorption mechanism is dominated by chemisorption[24–25], and the adsorption rate is influenced by the coordination of active sites on the material surface with metal ions[26]. The fitted equations for the quasi second-order kinetics of MML for Cu^{2+}, Zn^{2+} and Pb^{2+} were: $y = 0.09599x + 8.81861$, $y = 0.09333x + 10.01582$, and $y = 0.05103x + 5.02836$, respectively.

Intra-particle diffusion model

The adsorption process usually involves two main mechanisms: film diffusion and particle diffusion. In order to determine the way of metal ions entering the adsorbent material from the solution, the intra-particle diffusion model (Eq. 6) was used to determine the adsorption rate control steps and the results are shown in Fig. 3 and Table 2.

$$q_t = k_3 t^{1/2} + C \quad (6)$$

Where q_t is the amount of metal ions adsorbed at any moment t (mg/g), k_3 is the diffusion rate constant within the particle (min^{-1}), and C is the constant involving thickness and boundary layer. The larger the value of C, the greater the contribution

Table 2
Kinetic parameters of heavy metal ion adsorption on different samples: Lignite; MML.

Metal ion	Adsorption material	Quas first-order model			Quasi second-order model			Intra-particle diffusion model		
		K_1	q_e (mg/g)	R^2	K_2	q_e (mg/g)	R^2	K_3	C	R^2
Cu^{2+}	Lignite	0.00607	9.26020	0.98854	0.00072	10.1926	0.85585	0.73173	-1.65400	0.87331
	MML	0.01311	7.53811	0.99724	0.00104	10.4178	0.99906	0.87488	-1.72723	0.95551
Zn^{2+}	Lignite	0.00468	10.28394	0.98526	0.00070	9.7447	0.78164	0.68009	-1.56120	0.84320
	MML	0.01191	7.52736	0.99828	0.00087	10.7147	0.99925	0.85380	-1.78576	0.95279
Pb^{2+}	Lignite	0.01251	11.85742	0.96693	0.00038	19.0330	0.79657	1.47048	-3.53485	0.98318
	MML	0.01327	14.01561	0.98903	0.00052	19.5963	0.99463	1.63444	-3.37912	0.97145

of the boundary layer.

Figure 3 shows the linear relationship between q_t and $t^{1/2}$. Among them, the parameters of the intra-particle diffusion model for Cu^{2+}, Zn^{2+} and Pb^{2+} adsorption by lignite and MML are shown in Table 2. According to reports, if the plots are linear and pass through the origin, indicating that intra-particle diffusion is the only rate control step; if the linear plot of the fitted results does not pass through the origin, indicating that the adsorption rate is also controlled by other adsorption stages[27]. As can be seen in Fig. 5, the fitted results for the adsorption of Cu^{2+}, Zn^{2+} and Pb^{2+} by lignite and MML are linear and do not pass the origin, indicating that the rates of Cu^{2+}, Zn^{2+} and Pb^{2+} adsorption by lignite and MML are jointly controlled by multiple adsorption stages.

Analysis of the removal effects of lignite and MML on Cu^{2+}, Zn^{2+} and Pb^{2+}

The dynamic removal effects of lignite and MML on Cu^{2+}, Zn^{2+} and Pb^{2+} with time are shown in Fig. 4. The dynamic removal effects of both lignite and MML on Cu^{2+}, Zn^{2+} and Pb^{2+} showed a similar trend (Fig. 4). Metal ions were removed rapidly in the first 13 days, with removal rates of Cu^{2+}, Zn^{2+} and Pb^{2+} exceeding 95%, 92% and 97%, respectively, and then the removal rate gradually decreased from day 13 to day 22, and the removal rate was only about 10% at day 22. This phenomenon was attributed to the fact that there were enough binding sites on the surfaces of adsorbent lignite and MML for metal ions to occupy at the beginning of the reaction, which made the adsorption process easier. However, the number of effective adsorption sites on the surfaces of lignite and MML gradually decreased with time, which led to a decrease in the removal rate. During the whole dynamic removal cycle, the average removal rates of lignite for Cu^{2+}, Zn^{2+} and Pb^{2+} were 78.00%, 76.97% and 78.65%, respectively, and the average removal rates of MML for Cu^{2+}, Zn^{2+} and Pb^{2+} were 82.83%, 81.57% and 83.50%, respectively. Apparently, the adsorption capacity of MML for heavy metal ions increased due to the increase in specific surface area and pore volume[18].

Characterization Analysis

SEM analysis

The lignite and MML before and after the dynamic test were taken for SEM inspection, and the results are shown in Fig. 5. From Fig. 5(a) and (b), it can be seen that the surface of lignite is smooth, while the surface of MML is slightly rough, which is mainly due to the successful loading of Fe_3O_4 on the surface of lignite leading to the rough surface of MML. A large number of Fe_3O_4 particles scattered on the surface of lignite increased the specific surface area of the adsorbent material, which was beneficial to the removal of Cu^{2+}, Zn^{2+} and Pb^{2+} by the MML. As shown in Fig. 5(c) and (d), the surfaces of MML and lignite after adsorption of Cu^{2+}, Zn^{2+} and Pb^{2+} were very rough, and the granularity of the MML surface increased significantly, indicating that more heavy metal ions were adsorbed on the surface of MML.

XRD analysis

The XRD test results of lignite and MML before the dynamic test are shown in Fig. 5(e). Compared with lignite, the number of broad peaks in the XRD pattern of MML was reduced, indicating that the lignite changed from amorphous phase to crystalline phase during the magnetic modification process. The peaks at 2θ = 30.09°, 35.42°, 43.05°, 56.93° and 62.52° show (220), (311), (400), (511) and (440) diffraction planes, respectively, which are consistent with the standard XRD data of the cubic phase Fe_3O_4, and it can be inferred that Fe_3O_4 is successfully loaded onto the surface of lignite. The significant surface phase changes are consistent with SEM, which further verifies that the surface of MML becomes rougher due to the presence of Fe_3O_4. The rough surface of MML leads to an increase in specific surface area, which facilitates the adsorption of metal ions. The XRD results of lignite and MML after dynamic tests are shown in Fig. 5(f). Comparing the XRD plots of lignite and MML before and after the dynamic tests, it can be seen that no other crystal phases appeared in lignite and magnetically modified lignite after adsorption of Cu^{2+}, Zn^{2+} and Pb^{2+}, indicating that the adsorption process basically did not affect the crystal structures of lignite and MML.

FTIR analysis

The lignite and MML before and after the dynamic test were taken for FTIR detection, and the results are shown in Fig. 5(g) and (h). From Fig. 5(g) and (h), it can be seen that the peaks at 3400 cm^{-1} for lignite and MML are caused by O-H stretching vibrations of carboxylic acid groups, the peak at 2920 cm^{-1} is attributed to the presence of $-CH_2$ in the stretching of aliphatic compounds, and the peak at 1600 cm^{-1} is related to the stretching vibrations of carboxylic acid functional groups [19,29]. The disappearance of some peaks after magnetic modification of lignite, especially the generation of new peaks at 584 cm-1, is attributed to Fe-O stretching vibrations of Fe_3O_4 particles[30]. It shows that Fe_3O_4 was successfully loaded onto the lignite surface, which is consistent with the XRD results. After the adsorption of Cu^{2+}, Zn^{2+} and Pb^{2+} by dynamic tests, the band at 3384 cm^{-1} shifted to 3392 cm^{-1} for lignite, and the same was observed in the FTIR pattern of MML. The band at 3420 cm^{-1} shifted to 3426 cm^{-1} after the adsorption of metal ions by MML, which indicates the involvement of surface carboxylic acid ions in the adsorption of metal ions. The shape of the peak changed after the absorption of metal ions because the hydroxyl group of the carboxylic acid group stretched the vibration to metal ions. In addition, the band of MML at 584 cm^{-1} shifted to 580 cm^{-1}, indicating the interaction between Fe_3O_4 and metal ions during adsorption.

Conclusion

(1) The adsorption and removal rates of Cu^{2+}, Zn^{2+} and Pb^{2+} by MML are higher than those by lignite under the same metal concentration conditions. When the concentration of heavy metal ions in AMD solution is higher, MML has greater adsorption potential than lignite.

(2) The isothermal adsorption lines of lignite and MML for adsorption of Cu^{2+}, Zn^{2+} and Pb^{2+} are consistent with the Langmuir model, indicating that the adsorption is consistent with the unimolecular layer adsorption process. The adsorption processes of lignite for Cu^{2+}, Zn^{2+} and Pb^{2+} obeyed the quasi first-order kinetic model, indicating that the adsorption process was dominated by physical adsorption, and the fitted equations were: $y = 9.2602*(1-e^{-0.00607x})$, $y = 10.2839*(1-e^{-0.00468x})$, and $y = 11.8456*(1-e^{-0.01265x})$, respectively. The adsorption process of MML obeys the quasi second-order kinetic model, which indicates that the adsorption process is dominated by chemisorption and the adsorption rate is influenced by the coordination of active sites on the material surface with metal ions, and the fitted equations are: y = 0.09599x + 8.81861, y = 0.09333x + 10.01582, y = 0.05103x + 5.02836. The fitting results of intra-particle diffusion model show that the adsorption processes of lignite and MML are jointly controlled by multiple adsorption stages.

(3) The dynamic experimental results showed that the removal effect of MML on heavy metal ions was significantly better than that of lignite, where the average removal rates of lignite for Cu^{2+}, Zn^{2+} and Pb^{2+} were 78.00%, 76.97% and 78.65%, respectively, and the average removal rates of MML for Cu^{2+}, Zn^{2+} and Pb^{2+} were 82.83%, 81.57% and 83.50%.

(4) From SEM, XRD and FTIR tests, it can be seen that the magnetic modification process successfully loads Fe_3O_4 onto the surface of lignite, which destroyed the surface structure of lignite and made the surface morphology more rough. The adsorption process of MML on Cu^{2+}, Zn^{2+} and Pb^{2+} is related to the O-H stretching vibration of carboxylic acid ions and Fe-O stretching vibration of Fe_3O_4 particles.

Materials And Methods

Instruments

In this experiment, SEM (ZEISS-Sigma 500, GER) was used to observe the morphological characteristics and surface morphology of the samples. The phase and structure of the adsorbent were determined by XRD (Rigaku-SmartLab9, Japan). FTIR (Thermo Fisher-Nicolet iS5, USA) equipped with a potassium bromide spectrometer (KBr, FTIR grade) was used for the analysis of adsorbent materials. The flame ion spectrophotometer (Hitachi-Z2000, Japan) was used to detect the concentration of metal ions in the solution.

Raw materials

The lignite was purchased from Shanxi Fuhong Mineral Products Co., Ltd, crushed and ground through 60 mesh sieve, soaked and washed 2–3 times with deionized water, and dried at 80°C as the original material.

Preparation of MML

The chemical co-precipitation method is used to magnetically modify the lignite, that is, to load Fe_3O_4 magnetic particles on the surface of the lignite. The formation reaction formula of Fe_3O_4 is as follows.

$$Fe^{2+}+Fe^{3+}+8OH^{-}=Fe_3O_4\downarrow+4H_2O \quad (7)$$

According to the results of the previous experiments of the group[20], the ratio of Fe^{2+} to Fe^{3+} substance was set to 1:2, and a 200 mL, 0.7 mol/L Fe ion solution was prepared and placed in a constant temperature water bath at 60°C. After weighing 10 g of lignite into the Fe solution and stirring for 1 h under the action of an electric speed-controlled stirrer with a speed of 350 r/min, concentrated ammonia with a mass fraction of 25% was added drop by drop to pH 9, and stirring was continued for 1 h. The precipitate obtained from the reaction was washed repeatedly with deionized water to make the supernatant neutral, and the magnetic material was separated by a magnet and dried in a vacuum drying oven for 12 h to obtain the MML.

Experimental methods

Adsorption isotherm experiment

Cu^{2+}, Zn^{2+} and Pb^{2+} solutions with initial concentrations of 10 mg/L, 30 mg/L, 50 mg/L, 70 mg/L and 90 mg/L were prepared, and the pH of each solution was adjusted to 4. Lignite was added to the solution at a solid-liquid ratio of 1:250 (g/mL), and the sample was adsorbed by shaking at 150 r/min for 180 min and removed by pipetting. After filtered by 0.45 μm microporous membrane, the concentrations of Cu^{2+}, Zn^{2+} and Pb^{2+} remaining in the filtered solution were detected, and the removal rate and adsorption amount were calculated by using equations (2) and (3). The experimental procedure of MML adsorption isotherm was as described above.

$$E = \frac{C_0 - C_t}{C_0} \times 100\% \quad (8)$$

$$q_e = \frac{\left(C_0 - C_e\right) V}{M} \quad (9)$$

where E is the removal rate (%), C_0 is the initial mass concentration (mg/L), C_t is the mass concentration of the remaining metal ions in the solution at time t (mg/L), q_e is the adsorption amount at equilibrium (mg/g), C_e is the mass concentration of the

remaining metal ions in the solution at equilibrium (mg/L), V is the volume of the solution (L), and M is the mass of the adsorbent material (g).

Adsorption kinetics experiment

Each 250 mL, 30 mg/L of Cu^{2+}, Zn^{2+} solution and 250 mL, 50 mg/L of Pb^{2+} solution were added to a 500 mL conical flask, the pH of the solution was adjusted to 4 with 3% HNO_3, and 1 g of lignite was added. The conical flask was placed in an oscillator at 150 r/min for oscillatory adsorption, and samples were taken at intervals (5 min, 10 min, 15 min, 30 min, 60 min, 90 min, 120 min and 180 min) with a pipette, and the removed samples were filtered through a 0.45 μm microporous membrane to detect the remaining Cu^{2+}, Zn^{2+} Pb2 $^{+}$ concentration in the solution, and the removal rate and adsorption amount were calculated respectively. The experimental procedure of magnetic modified lignite adsorption kinetics was as described above.

Dynamic experiment

Acrylic columns 1# and 2# with an inner diameter of 40 mm and a height of 250 mm were set up and filled with lignite and magnetically modified lignite, respectively. The dynamic columns were arranged with 25 mm high glass beads of 3–5 mm in diameter at the top and bottom, 100 mm high lignite in the middle of 1# acrylic column, and 100 mm high magnetically modified lignite in the middle of 1# acrylic column. According to the static test results, a solution with pH = 4, Cu^{2+}, Zn^{2+} and Pb^{2+} concentrations of 30 mg/L, 30 mg/L and 50 mg/L was prepared as the laboratory simulated AMD test solution with reference to the measured water quality index of AMD in a mining area in Huludao City, Liaoning Province. The overall operation mode was "lower inlet and upper outlet" continuous operation, and the inlet flow rate was adjusted to 0.556 mL/min by peristaltic pump and flowmeter, and the experimental setup is shown in Fig. 6. The two sets of dynamic columns were operated continuously at room temperature for 20 days, and the samples were taken every 12 h. The samples were filtered through 0.45 μm microporous membrane and the remaining Cu^{2+}, Zn^{2+} and Pb^{2+} concentrations in the solution were detected.

Declarations

Competing interests

Te authors declare no competing interests.

Data Availability

All data generated or analysed during this study are included in this published article.

Author contributions statement

J.D., and Z.R. wrote this paper. J.D., Z.R., and S.Z. fnished the water quality analysis. J.D., Z.R., and S.Z. performed the long-term experiment. All authors reviewed the manuscript.

References

1. Akcil, A. & Koldas, S. Acid Mine Drainage (AMD): causes, treatment and case studies. *Journal of Cleaner Production*. **14,** 1139-1145. https://doi.org/10.1016/j.jclepro.2004.09.006 (2006).
2. Akinpelu, E. A., Ntwampe S. K.O., Fosso-Kankeu, E., Nchu, F., Angadam, J. O. Performance of microbial community dominated by Bacillus spp. in acid mine drainage remediation systems: A focus on the high removal efficiency of SO_4^{2-}, Al^{3+}, Cd^{2+}, Cu^{2+}, Mn^{2+}, Pb^{2+}, and Sr^{2+}. *Heliyon*. **7(6),** e07241, https://doi.org/10.1016/j.heliyon.2021.e07241 (2021).
3. Ge, F., Li, M. M., Ye, H. & Zhao, B. X. Effective removal of heavy metal ions Cd^{2+}, Zn^{2+}, Pb^{2+}, Cu^{2+} from aqueous solution by polymer-modified magnetic nanoparticles. *Journal of Hazardous Materials*. **211-212,** 366-372. https://doi.org/10.1016/j.jhazmat.2011.12.013 (2012).
4. Magagane, N., Masindi, V., Ramakokovhu, M. M., Brendon, S. M. & Lilith, M. K. Facile thermal activation of non-reactive cryptocrystalline magnesite and its application on the treatment of acid mine drainage. *Journal of environmental*

management. **236,** 499-509. https://doi.org/10.1016/j.jenvman.2019.02.030 (2019).

5. Matlock, M. M., Howerton, B. S. & Atwood, D. A. Chemical precipitation of heavy metals from acid mine drainage. *Water Research*. **36,** 4757-4764. https://doi.org/10.1016/S0043-1354(02)00149-5 (2002).
6. Nogueira, E. W., Godoi, L., Yabuki, L., Brucha, G. & Damianovic, M. Sulfate and metal removal from acid mine drainage using sugarcane vinasse as electron donor: Performance and microbial community of the down-flow structured-bed bioreactor. *Bioresource Technology*. **330,** 124968, https://doi.org/10.1016/j.biortech.2021.124968 (2021).
7. Sheoran, A. S. & Sheoran, V. Heavy metal removal mechanism of acid mine drainage in wetlands: A critical review. *Minerals Engineering*. **19,** 105-116. https://doi.org/10.1016/j.mineng.2005.08.006 (2006).
8. Li, R., Liu, Y., Lan, G. & Zhang, L. Pb(□) adsorption characteristics of magnetic GO-hydroxyapatite and the contribution of GO to enhance its acid resistance. *Journal of Environmental Chemical Engineering*. **9,** 105310, https://doi.org/10.1016/j.jece.2021.105310 (2021).
9. Zhao, R. et al. Branched polyethylenimine grafted electrospun polyacrylonitrile fiber membrane: a novel and effective adsorbent for Cr(VI) remediation in wastewater. *Journal of Materials Chemistry A*. DOI: 10.1039/C6TA09784G (2016).
10. Zhou, G. Y., Luo, J.M., Liu, C. B., Chu, L. & Crittenden, J. Efficient heavy metal removal from industrial melting effluent using fixed-bed process based on porous hydrogel adsorbents. *Water Research*. **131,** 246-254. https://doi.org/10.1016/j.watres.2017.12.067 (2018).
11. Zhao, T. T. et al. Mechanism study of Cr(III) immobilization in the process of Cr(VI) removal by Huolinhe lignite. *Fuel Processing Technology.* **152,** 375-380. https://doi.org/10.1016/j.fuproc.2016.06.037 (2016).
12. Smilek, J., Sedláček, P., Kalina, M. & Klučáková, M. On the role of humic acids' carboxyl groups in the binding of charged organic compounds. *Chemosphere*. **138,** 503-510. https://doi.org/10.1016/j.chemosphere.2015.06.093 (2015).
13. Murata, S., Hosokawa, M., Kidena, K. & Nomura, M. Analysis of oxygen-functional groups in brown coals. *Fuel Processing Technology*. **67(3),** 231-243. https://doi.org/10.1016/S0378-3820(00)00102-8 (2000).
14. Mohan, D. & Chander S. Removal and recovery of metal ions from acid mine drainage using lignite—A low cost sorbent. *Journal of Hazardous Materials*. **137(3),** 1545-1553. https://doi.org/10.1016/j.jhazmat.2006.04.053 (2006).
15. Yang, Q. W., Zhang, J. J., Bao, X. L. & Hua, D. L. Study on improving cadmium adsorption capacity of lignite modified by nitric acid oxidation lignite. *Journal of Henan Agricultural University*. **53(3),** 426-433+447. (2019).
16. Zhang, H. C., Wang, Z. F., Li, J. Y., Ye, X. Q. & Liu, H. B. Studies on adsorption characteristics of lignite activated by sulphonation or alkalization for heavy-metal ions[J]. *Envitonmental Chemistry*. **18(5),** 482-487 (1999).
17. Di, J. Z. et al. Experimental study on adsorption of Cu^{2+} and Zn^{2+} in Acid Mine Drainage by modified lignite. *Coal Science and Technology*. https://kns.cnki.net/kcms/detail/11.2402.td.20201207.1610.002.html
18. Cheng, Z. H. et al. Preparation of magnetic Fe_3O_4 particles modified sawdust as the adsorbent to remove strontium ions. *Chemical Engineering Journal*. **209,** 451-457. https://doi.org/10.1016/j.cej.2012.07.078 (2012).
19. Wang, W. P. Research on the adsorption of Cu^{2+}, Pb^{2+} and Cd^{2+} ions onto magnetical modified sepiolite and their adsorption mechanisms. Xiangtan University, 2012.
20. Di, J. Z., Lin, X. & Dong, Y. R. Preparation of Magnetically Modified Mineral Materials and Their Adsorption Kinetics. *Non-Metallic Mines*. **42(6),** 86-89 (2019).
21. Albadarin, A. B. et al. Kinetic and Thermodynamics of Chromium Ions Adsorption onto Low-cost Dolomite Adsorbent. *Chemical Engineering Journal*. **179,** 193-202. https://doi.org/10.1016/j.cej.2011.10.080 (2012).
22. Chethan, P. D. & Vishalakshi, B. Adsorption Efficiency of Cr(VI) by Ethylene-1, 2-Diamine-6-Deoxychitosan. *Separation Science and Technology*. **50(8),** 1158-1165. https://doi.org/10.1080/01496395.2014.967405 (2015).
23. Kavitha, D. & Namasivayam, C. Experimental and kinetic studies on methylene blue adsorption by coir pith carbon. *Bioresour Technol*. **98(1),** 14-21. https://doi.org/10.1016/j.biortech.2005.12.008 (2007).
24. Zhao, H. X. & Lang, Y. H. Adsorption behaviors and mechanisms of florfenicol by magnetic functionalized biochar and reed biochar. *Journal of the Taiwan Institute of Chemical Engineers*. **88,** 152-160. https://doi.org/10.1016/j.jtice.2018.03.049 (2018).

25. Hameed, B. H., Salman, J. M. & Ahmad, A. L. Adsorption isotherm and kinetic modeling of 2,4-D pesticide on activated carbon derived from date stones. *Journal of hazardous materials*. **163(1),** 121-162. https://doi.org/10.1016/j.jhazmat.2008.06.069 (2009).
26. Bai, J. R. et al. Kinetics and thermodynamics of adsorption of heavy metal ions onto fly ash from oil shale. *Journal of Fuel Chemistry and Technology*. **39(5),** 378-384 (2011).
27. Wang, X. et al. Isothermal Adsorption Characteristics and Kinetics of Cr Ions onto Ettringite. *Journal of Wuhan University of Technology(Materials Science)*. **34(3),** 587-595. https://doi.org/10.1007/s11595-019-2092-0 (2019).
28. Hong, Y. K. et al. Bottom Ash Modification via Sintering Process for Its Use as a Potential Heavy Metal Adsorbent: Sorption Kinetics and Mechanism. Materials. **14(11),** 3060, https://doi.org/10.3390/ma14113060 (2021).
29. Kong, Q. P., Wei, J. Y., H, Y. & Wei, C. H. Fabrication of terminal amino hyperbranched polymer modified graphene oxide and its prominent adsorption performance towards Cr(VI). *Journal of Hazardous Materials*. **363,** 161-169. https://doi.org/10.1016/j.jhazmat.2018.09.084 (2018).
30. Deng, S. B., Liu, H., Zhou, W., Huang, J. & Yu, G. Mn-Ce oxide as a high-capacity adsorbent for fluoride removal from water.. *Journal of Hazardous Materials*. **186(2-3),** 1360-1366. https://doi.org/10.1016/j.jhazmat.2010.12.024 (2011).

Figures

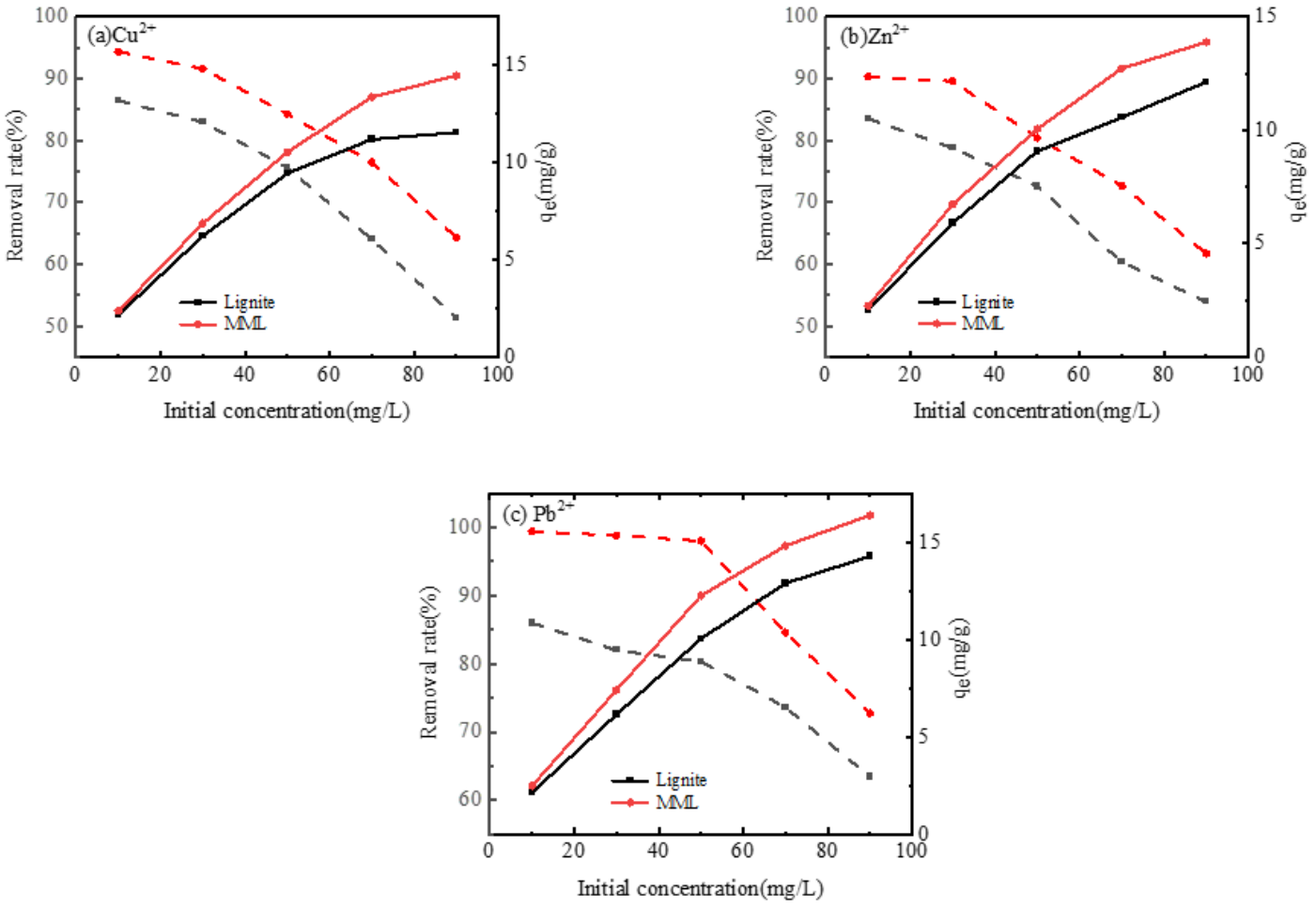

Figure 1

Relationship between initial concentration and adsorption effect using sorbent dose of 1 g/mL. (a) Cu2+, (b) Zn2+, (c)Pb2+.

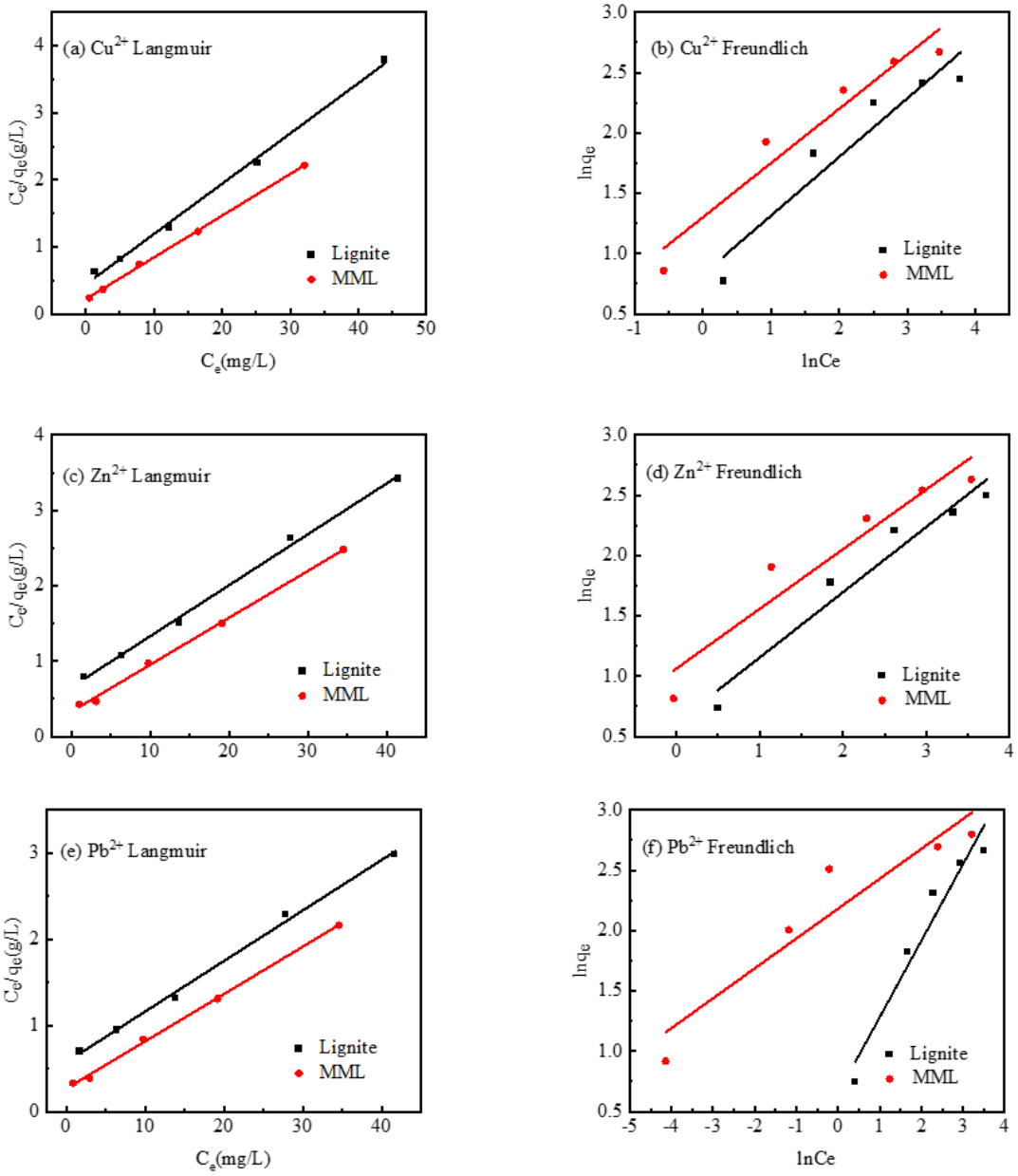

Figure 2

Linear plots of adsorption isotherms of heavy metal ion adsorption on different samples: Lignite; MML. (a) Cu2+Langmuir, (b) Cu2+Freundlich, (c) Zn2+Langmuir, (d) Zn2+Freundlich, (e)Pb2+Langmuir, (f) Pb2+ Freundlich

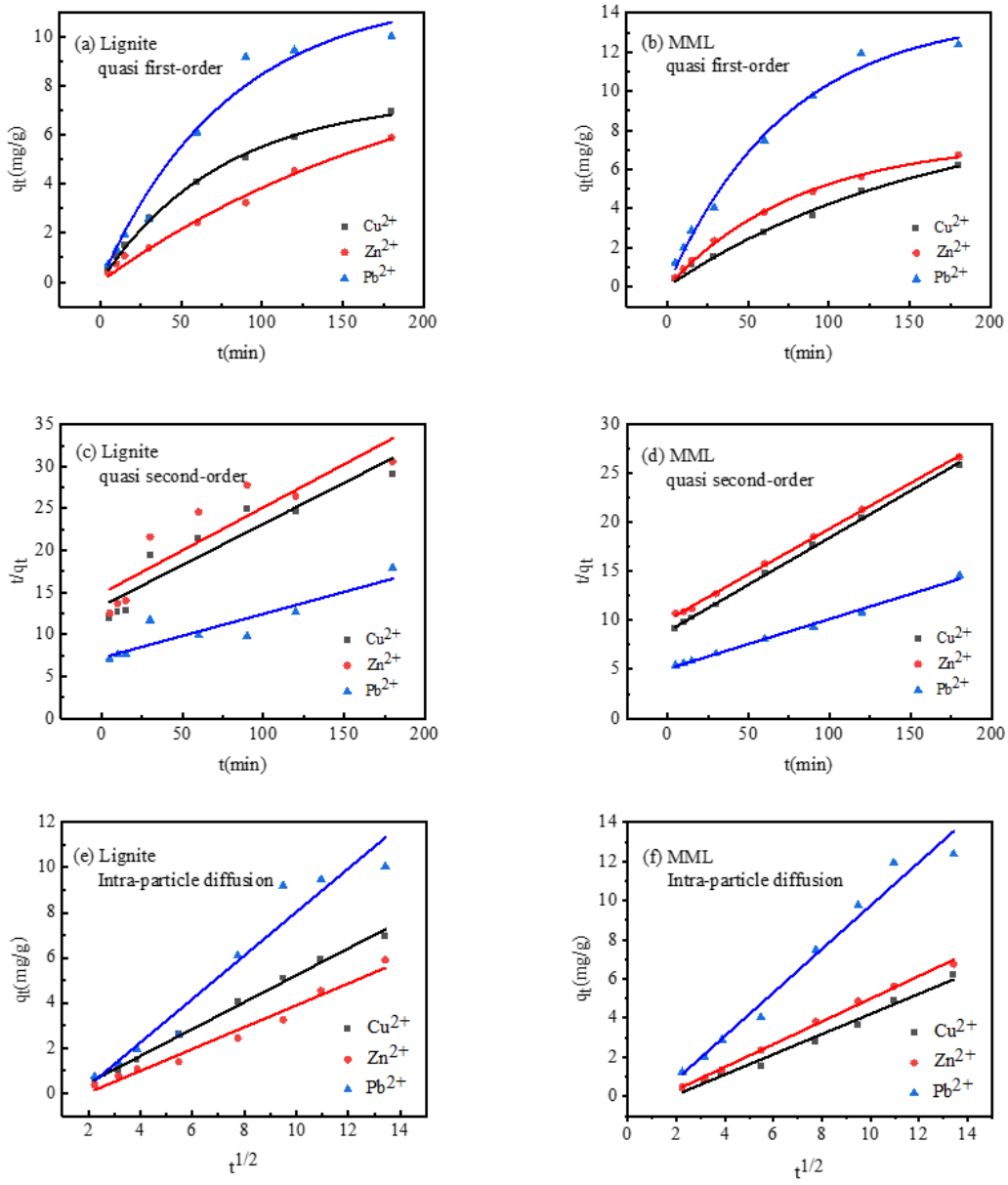

Figure 3

dsorption kinetics of heavy metal ion adsorption on different samples: Lignite; MML.

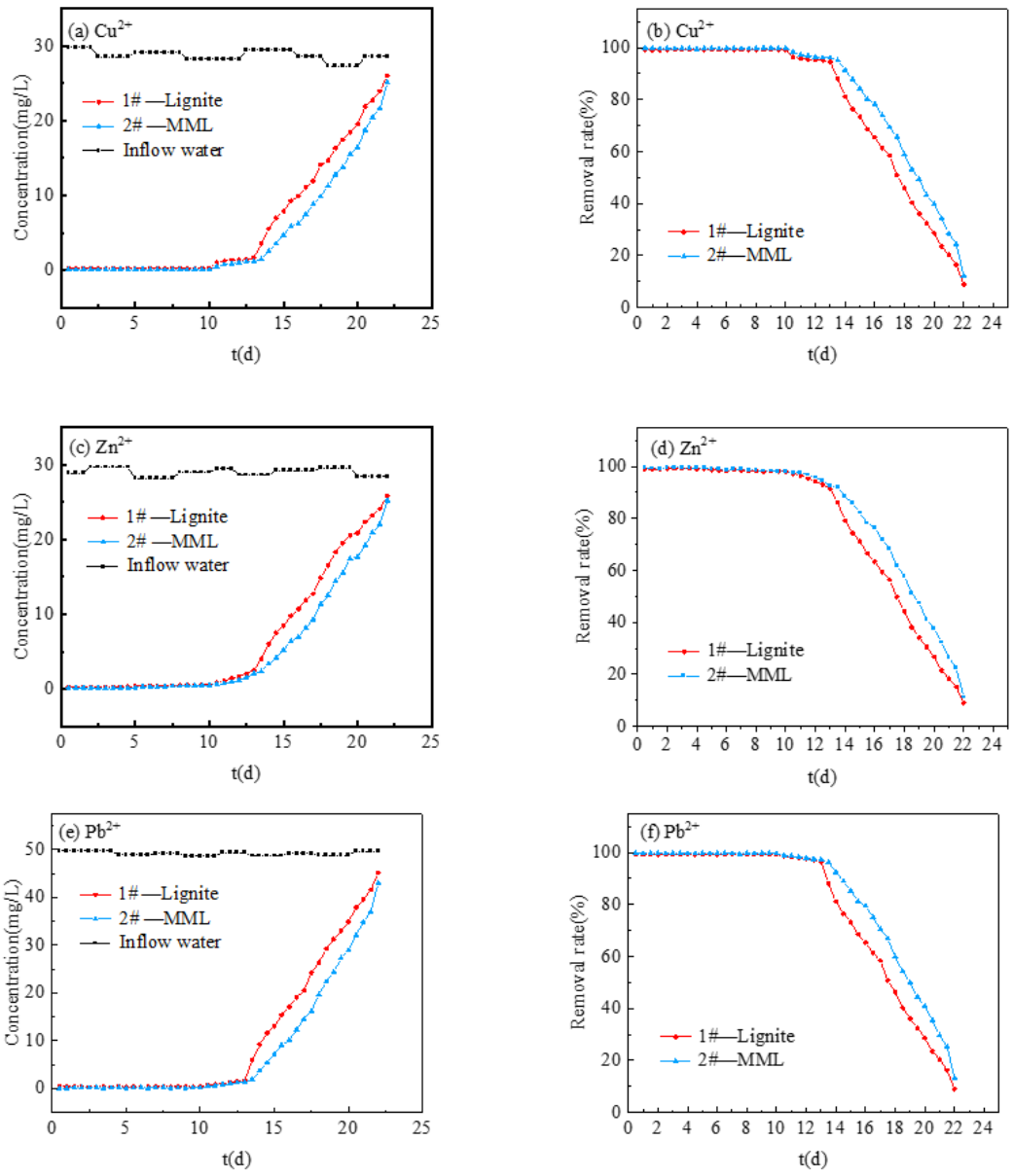

Figure 4

Removal effect of heavy metal ion. (a) Cu2+, (b) Cu2+, (c) Zn2+, (d) Zn2+, (e) Pb2+, (f) Pb2+.

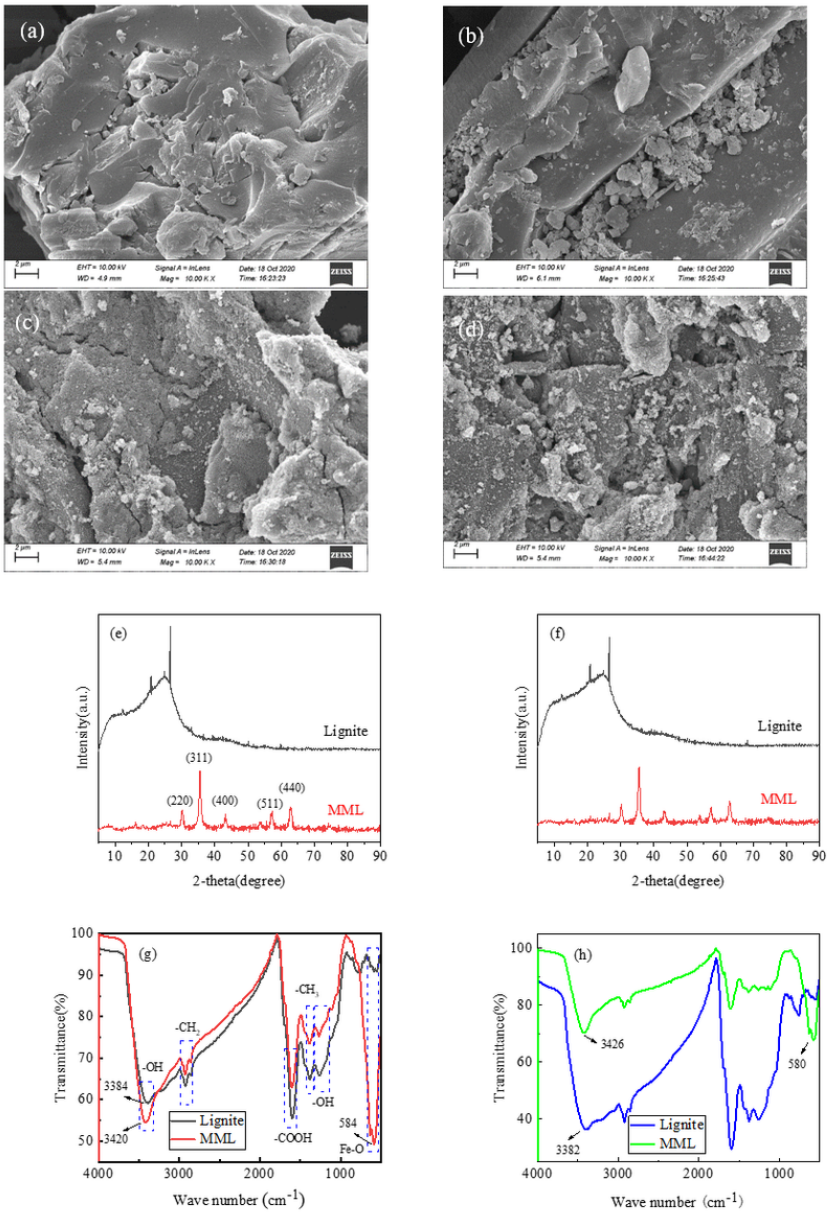

Figure 5

SEM images of (a) Lignite, (b)MML, (c) Lignite after heavy metal ion adsorption, (d)MML after heavy metal ion adsorption. XRD patterns of Lignite and MML: (e) Before adsorption, (f) After adsorption. FTIR spectra of Lignite and MML: (g) Before adsorption, (h) After adsorption.

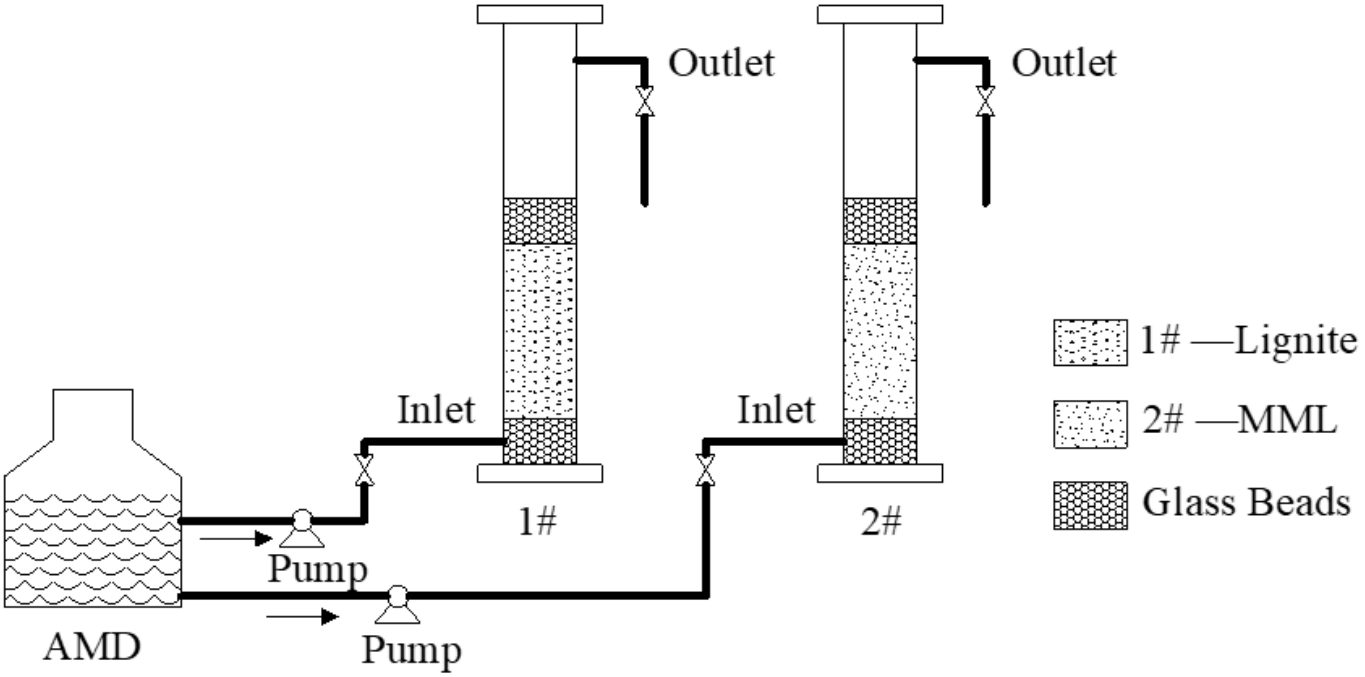

Figure 6

Dynamic test running device diagram.